ELSEVIER

Catalysis Today 79–80 (2003) 511–520

CATALYSIS TODAY

www.elsevier.com/locate/cattod

Monolithic integrated fuel processor for the conversion of liquid methanol

M. Schuessler*, M. Portscher, U. Limbeck

Ballard Power Systems AG, 73230 Kirchheim/Teck-Nabern, Germany

Abstract

Using a liquid fuel to run a fuel cell system becomes more attractive, when a simple and robust fuel processor can be developed. Conversion of a liquid methanol/water-mixture needs a series of process steps to supply hydrogen to a fuel cell. Based on an approach using new material these processes are combined in an integrated fuel processor (IFP). We apply technologies from powder metallurgy like pressing and sintering, to fix catalyst powder and to shape complex functional structures. As a consequence of the new material approach, the IFP can be built as a monolith without any sealing. The good isotropic heat conductivity helps to thermally couple the processes. Experimental results on a level of about 20 l of hydrogen per minute demonstrate the feasibility of the concept. Supported by modelling, alternative schemes of reactor design indicate potential for optimisation.

Keywords: Fuel processor; Microreactor; Multifunctional reactor; Catalyst fixation; Vaporisation; Methanol; CO-oxidation

1. Introduction

Liquid fuels are attractive for fuel cell systems because of their high energy storage density. Nevertheless, they require fuel processing to release the chemically bound hydrogen. The fuel processor adds complexity, cost and weight when compared to the system running on gaseous hydrogen [1].

Subject of the work presented here is to design a very simple and robust fuel processor for the production of hydrogen by reforming of methanol. A simple and robust fuel processor would enable to combine the advantages noted above: high energy storage density of the fuel combined with high system power density and low system cost.

Methanol fuel processing needs a comparatively low process temperature for reforming. However, the general design and materials of the fuel processing sections, as well as the operation strategies are often similar to the ones used for methane or diesel, that means the processes are mainly carried out in a series of single controlled reactors made of steel [2]. In the approach chosen here we take advantage of the benefits arising from methanol. The thermal coupling of the selective CO-oxidation with the endothermic reforming is already well established [3]. Moreover, we try to integrate all process steps that are on similar temperature levels in one monolithic integrated fuel processor (IFP). Important advantages following from this approach are: simpler start-up and dynamic control of the system, lower cost and easy replacement of the catalytic sections.

The processes combined in the IFP are: vaporisation of a mixture of methanol and water (1), followed by reforming (2) or autothermal reforming (3). Consequently selective oxidation of carbon monoxide (4) accompanied by the burning of hydrogen (5) are

* Corresponding author.
E-mail address: martin.schuessler@ballard.com (M. Schuessler).

0920-5861/03/$ – see front matter
doi:10.1016/S0920-5861(03)00076-2

Nomenclature

b	width of the reactor (m)
c	concentration (% respectively ppm)
$\dot{F}_{SI}$	flux of side feed of component i (mol/(s m))
ΔH°	standard heat of process (kJ/mol)
k_{inh}	rate constant (mol/(s g_{Pt} $bar^{1.5}$))
k_4	rate constant (mol/(s g_{Pt} $bar^{1.5}$))
k_5	rate constant (mol/(s g_{Pt} $bar^{0.17}$))
k_{6a}	rate constant (mol/(s g_{Pt}))
k_{6b}	rate constant (s g_{Pt}/(mol bar))
K_{CO}	sorption constant (1 bar^{-1})
$\dot{n}_i$	molar flux of component i (mol s^{-1})
p_i	partial pressure of component i at catalyst (bar)
$p_{i,\,bulk}$	partial pressure of component i in the bulk (bar)
r_j	catalyst related rate for the reaction j (mol/(s g_{Pt}))
R	gas constant (J/(mol K))
T	temperature (K)
z	length (m)

Greek letters

β_i	mass transfer coefficient of component i (m s^{-1})
λ_{H_2O}	ratio of water to methanol (–)
ν_{ij}	stoichiometric coefficient of component i in reaction j (–)
ρ_{cat}	catalyst density (g_{Pt} m^{-2})

conducted. As a side reaction for all noted catalytic processes the reverse water-gas shift (RWGS) reaction (6) is always taking place. For the start-up of the system also the complete oxidation of methanol (7) is relevant. Table 1 shows an overview of the equations, the respective temperature range and the standard molar heat of the processes involved.

A heat conducting structure is necessary to thermally combine the processes noted above. We use techniques coming from powder metallurgy, like pressing and sintering of powder mixtures, to hold the catalyst, shape the functional sections of the fuel processor and to conduct the heat between the processes. The powder technique was developed to supply a reactor, that is nearly free of gradients to withstand dynamic requirements of automotive application [4,5]. In general lack of maldistribution and macroscopic gradients for mass and heat is a characteristic of microreactors [6]. In terms of power level, our reactor is more than an order of magnitude above most other approaches to integrated fuel processing [7]. Nevertheless, it also relies on the principles of microreactors noted above.

All microreactor concepts have to deal with the question, how to fixate the respective catalysts [8,9], especially when the traditional large scale solution is a packed bed of pellets. It was already shown that the powder technique solves the problem of contacting and fixing a relatively high mass of catalyst necessary for reforming [5]. While setting up the IFP, here we will investigate, which other benefits in manufacturing, design and cost can be derived from the powder techniques.

2. Experimental/fabrication of the IFP

The different materials leading to the later reactor are added as powders in a die. The reforming section is built from a mixture of a CuZnO-catalyst and copper powder. Copper is used as a matrix building material

Table 1
Overview of processes integrated into the IFP

Process		T-range of operation (°C)	ΔH° (kJ/mol)
$MeOH/H_2O$ (liquid) → $MeOH/H_2O$ (gaseous)	(1)	0–100	38/44
$CH_3OH + H_2O \rightarrow CO_2 + 3H_2$	(2)	230–300	50
$CH_3OH + 0.1O_2 + 0.8H_2O \rightarrow CO_2 + 2.8H_2$	(3)	230–300	0
$CO + 0.5O_2 \rightarrow CO_2$	(4)	150–300	−283
$H_2 + 0.5O_2 \rightarrow H_2O$	(5)	150–300	−242
$CO_2 + H_2 \rightarrow CO + H_2O$	(6)	150–300	41
$CH_3OH + 1.5O_2 \rightarrow CO_2 + 2H_2O$	(7)	0–300	−676

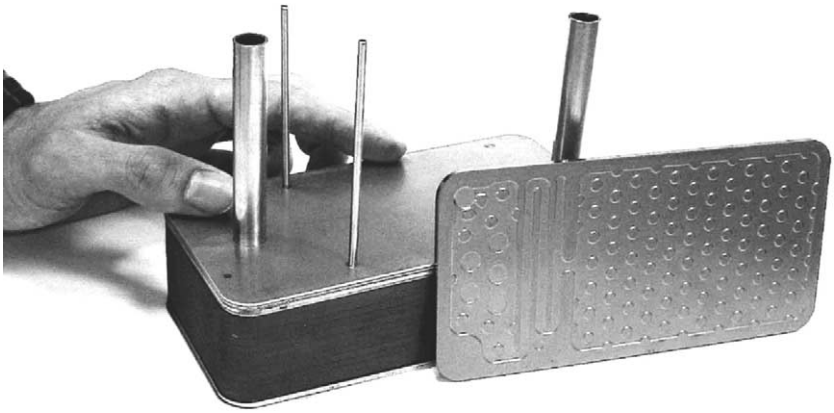

Fig. 1. Single plate and stack with endplates building a monolithic IFP producing up to 20 l of hydrogen per minute from liquid methanol/water-mixture.

because of its high heat conductivity and low melting point (1083 °C). Due to the low melting point, it is possible to join the copper particles by sintering [10] at moderate temperatures (500–700 °C). Most other metals would require temperatures that harm the catalytic activity. The copper powder is a dendritic type (type FFL, MicroMet), which clamps together and builds a porous body sufficiently stable even before sintering. The CuZnO-catalyst is a non-commercially available product developed by BASF. It is used in a particle size fraction 100–300 μm.

Copper or aluminium powder alone as inert matrix material serve as material for the other functional sections, like channels, edges or diffusion layers. The different powders are filled into separated zones of a die and pressed at room temperature with a pressure of 100 MPa. The porosity and characteristics for gas transport are adjusted by the choice of powder and the degree of compression in the respective zone.

After pressing, certain sections of the plate have to be coated with a Pt-catalyst layer. Pt-catalyst is necessary for the exothermic oxidation (Eqs. (5)–(7)). The alumina supported Pt (Johnson Matthey, non-commercial) is milled and spray-coated as a suspension in an alumina based binder (Sasol/Condea).

Porous preformed cylinders (7 mm diameter, 1 mm height), made of stainless steel or ceramic, are added to accommodate the vaporisation. These pieces are placed on every plate before the plates are piled to form a modular reactor. The stack and one plate can be seen in Fig. 1.

The next step of manufacturing is sintering the stack. In this step the matrix particles join at their contact surfaces, leading to mechanically stable plates and a tight connection between the piled plates without any additional sealing. During the sinter process also the binding of the coating takes place and the endplates (Fig. 1) are joined to the stack. Furthermore, “baking” leads to good heat conductivity from one plane to the next via mechanically supporting interconnections and the joined region of the edges.

3. Design of the IFP

Fig. 2 shows the functional sections on a single plate of the IFP [11].

The methanol/water-mixture is injected into the vaporisation units and the emerging gas enters the air stream flowing around the vaporiser cylinders. In the subsequent section the two streams are mixed before they reach the region of autothermal reforming. Here the mixture is converted while passing through the porous plate, that contains the catalyst. After passage through the porous plate the product gas is collected again, a second air flow is added and mixed. Finally the section of CO-oxidation is reached, which is located on the backside of the vaporisation. There are two major heat sinks in the system of combined processes. The heat of vaporisation is delivered by the oxidation of carbon monoxide and hydrogen as shown in Fig. 2. The second heat flow takes place within

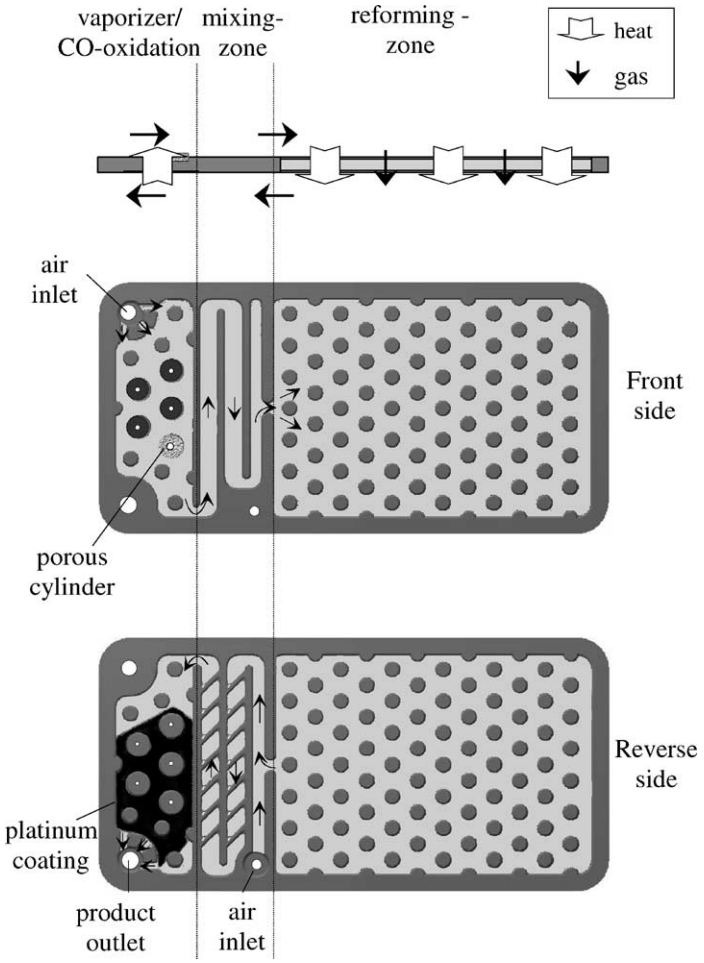

Fig. 2. Functional sections on a single plate of the IFP.

the region of autothermal reforming. While passing through the plate, the oxygen is consumed first [5] and the subsequent reforming (Eq. (2)) is supplied by heat conduction along the distance of about 2 mm. The overall reaction in the porous plate is thermally balanced. The short distance from heat source to its sink is a basic design principle for the ATR-region. The temperature gradient perpendicular to the plate is about 10 K. In the planar direction a diffusion layer on top of the ATR-catalyst zone makes sure, that the oxidation (Eq. (7)) is equally distributed over the plane. Conducting the same reactions e.g. on a coated plate with the gas flow in parallel, the planar temperature gradient would be more than 100 K [4], and diffusion would have to overcome an extended hydrodynamic boundary layer. The diameter of the pores leading through the plate is about 2 μm and porosity is about 60%. Therefore the flow is mainly laminar, and diffusion length to the catalyst particle is extremely small. The excellent isothermal conditions together with the short diffusion distances in the porous plate guarantee optimal transport of heat and mass. As a consequence high load and long lifetime can be achieved. The pressure drop necessary to flow through the plate is a design parameter. It depends on the compression of the porous structure and, of course, on the thickness of the plate. For full load, pressure drop can be limited to 200 mbar.

The process of vaporisation is special, as the process temperature is significantly lower compared to the

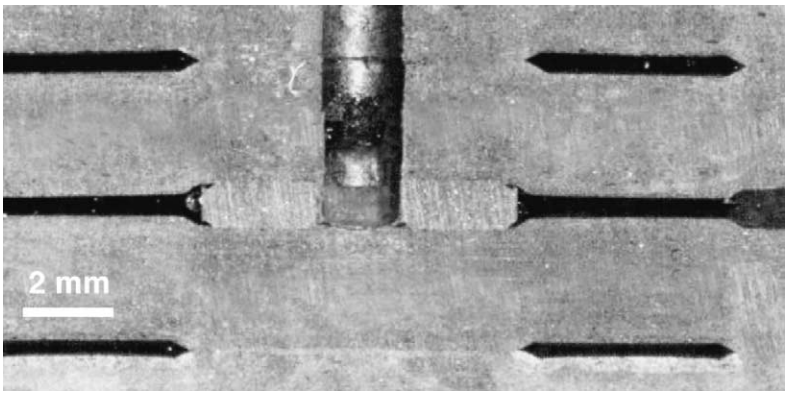

Fig. 3. Cross-section of the porous vaporisation disk clamped between two plates. The liquid is injected by a capillary (not shown) that enters through the bore.

other processes (Table 1). Nevertheless, the process was also integrated, since it offers a huge heat sink. The difference between the general operation temperature in the plates and the temperature of vaporisation necessitates a special approach to the design of the section. In Fig. 3 cylindrical porous bodies between two plates can be seen. Via a capillary (not shown) the liquid fuel is injected into such a porous disk. These disks are clamped, not joined, between the plates to ensure thermal contact on the one hand, but also to allow thermal expansion on the other hand [12]. That means, the disks are mechanically free when it comes to thermal expansion. FEM analysis proved the strong need for such a concept, otherwise lifetime would be very limited due to mechanical stress.

The single plates are piled alternately face up and face down. So two plates are always building an educt or product flow field between them. For the prototype demonstrated in Fig. 1 10 plates were sintered together.

The two endplates are also joined to the stack during the sintering process. This leads to a monolithic body completely free of sealings with piping ends ready for connection (Fig. 1).

For such a highly parallel reactor concept, equal distribution of the educts among the different cells is a crucial point. For both, the fuel and air, this is guaranteed by very small deviations from the mean pressure drop of the cells. The pressure drop of the passage through the plates differs less than 3% due to reproducible manufacturing methods. For the liquid the identical lengths of the capillaries ensures the equal distribution [13].

The edge of the plates is sufficiently impermeable, because it is strongly compressed. As a consequence a housing for the stack is not necessary. Nevertheless, a thermal insulation may be applied to decrease heat losses and to protect neighbouring components. The whole IFP shown in Fig. 1 has a mass of 1.8 kg and a volume of 0.5 l. A thermocouple measures the stack temperature. With the help of this sensor the air flow to the IFP is controlled, ensuring a stable operation.

4. Experimental results and discussion

The experimental characterisation of the IFP started with a gaseous feed from an electric vaporiser in the test bench. That means, only the autothermal reforming is active, whereas vaporisation and CO-oxidation are not used. The feed of methanol was 15 mol/h, the ratio of water to methanol λ_{H_2O} was 1.0, back pressure was 1.5 bar(a) and the temperature of the IFP was kept at 280 °C. The composition of the product gas (dry) is demonstrated in the left part of Fig. 4 (balance is nitrogen).

These are the typical concentrations with c(CO) somewhat below thermodynamic equilibrium. Due to heat losses of the small reactor, the concentration of hydrogen is lower than the 65%, which would be calculated from the Eqs. (3) and (6). The right part

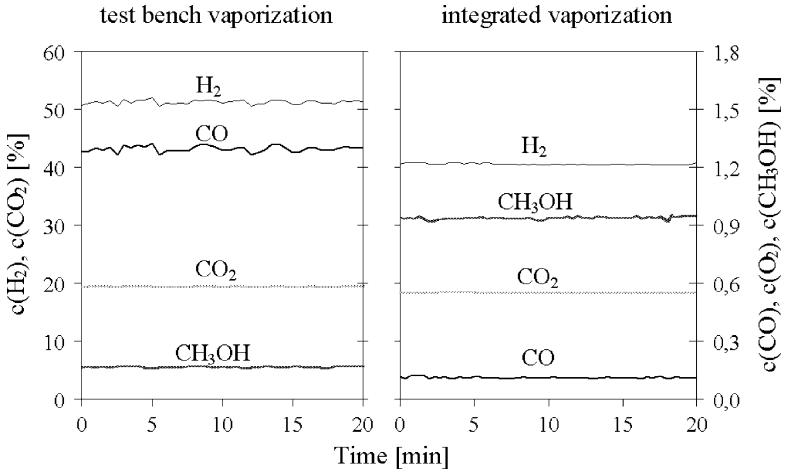

Fig. 4. Product concentrations (dry) of the IFP with external and internal vaporisation (methanol feed: 15 mol/h, $\lambda_{H_2O} = 1.0$, $T = 280\,^{\circ}C$, $p_{out} = 1.5$ bar(a)).

of Fig. 4 shows the results with integrated vaporisation and CO-oxidation active. All concentrations are lower compared to the left side, because more air is necessary to thermally balance the vaporisation and therefore nitrogen dilutes the reformate. The amount of CO is significantly reduced proofing the functionality of the CO-oxidation section. The reason for the increased concentration of methanol probably is a small bypass through the plate separating vaporisation and CO-oxidation in the front region. It is notable to find the curves of the concentrations over time to be smoother with the integrated vaporiser compared to the curves with the test bench vaporiser. This indicates that only vaporised feed leaves the porous cylinders in the front section.

Fig. 5 presents the product composition when the feed rate is varied. The feed rate of Fig. 4 corresponds to a hydrogen product flow of 11×10^{-3} mol s^{-1}.

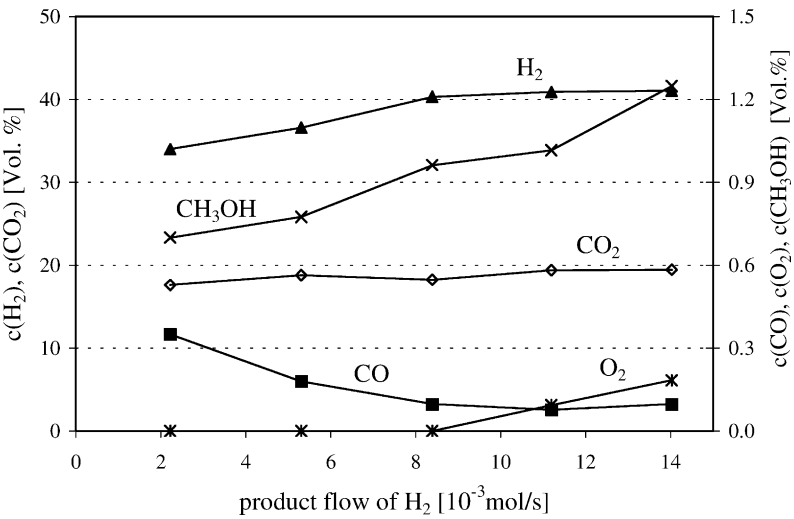

Fig. 5. Product concentrations (dry) of the IFP as a function of load with internal vaporisation and CO-oxidation active ($\lambda_{H_2O} = 1.0$, $T = 280\,^{\circ}C$, $p_{out} = 1.5$ bar(a)).

Here also a small amount of oxygen is found in the product, indicating that the oxidation section starts being overloaded. With decreasing feed rate the heat loss and thus the nitrogen dilution grows and the oxidation section is handicapped by the RWGS reaction. The fact that the methanol in the product approaches a value much higher than zero strengthens the assumption of a bypass. During the measurements the temperature distribution in the autothermal section was very even with maximum differences below 10 K.

The start-up of the reactor from room temperature is conducted according to the following procedure: liquid methanol/water-mixture is dosed into vaporisation section as usual, but the flow of air into the section is much higher than necessary according to Eq. (7). The air takes up vaporised methanol and water. Now the oxidation in the subsequent catalytic zones can start, especially the Pt-coated reverse side of the vaporisation section produces heat. This heat is supplied to the vaporisation accelerating the whole process. After about 10 min the IFP can be switched to normal operation by simply reducing the air stoichiometry.

5. Simulation of alternative contacting patterns

5.1. The model

The powder technology opens the possibility to have side feed of reactants through extended porous layers. For the selective oxidation of CO (Eq. (4)), these alternative contacting patterns are compared by computer simulation. Fig. 6 differentiates between four cases of contacting patterns for reformate and air. The first case can be regarded as the reference case, because it represents the pattern which is shown in Fig. 2. Reformate and air are mixed before entering the reaction zone of selective oxidation. In the second case reformate is generated in the porous reformer catalyst that acts also as carrier for the coated porous Pt-catalyst. This represents a side feed of the reformate while air is still fed at the beginning of the reactor. In the third case of Fig. 6, the air is fed along the reactor as side feed from above while reformate is again generated at the bottom of the reactor. The last case consists of a side feed of air and a reformate feed stream at the beginning of the reactor.

In order to obtain fundamental statements concerning the reactor design a simplified isotherm one-dimensional model of the reactor was developed. Assuming plug flow, the i balance equations for the components CO, H_2O, O_2, CO_2, H_2, CH_3OH and N_2 are

$$\frac{d\dot{n}_i}{dz} = \dot{F}_{SI} + b\rho_{cat}\sum_{j=4}^{6} \nu_{ij} r_j \tag{8}$$

In Eq. (8), $\dot{n}_i$ denotes the molar flux (mol s^{-1}) of component i, $\dot{F}_{SI}$ the flux of side feed (mol/(s m)), b the width of the reactor (m), ρ_{cat} the catalyst density (g_{Pt} m^{-2}), ν_{ij} the stoichiometric coefficient of component i in reaction j and r_j the catalyst related rate for the reaction j (mol/(s g_{Pt})).

The reaction scheme for selective oxidation consists of the three parallel reactions: (4)–(6). Reaction

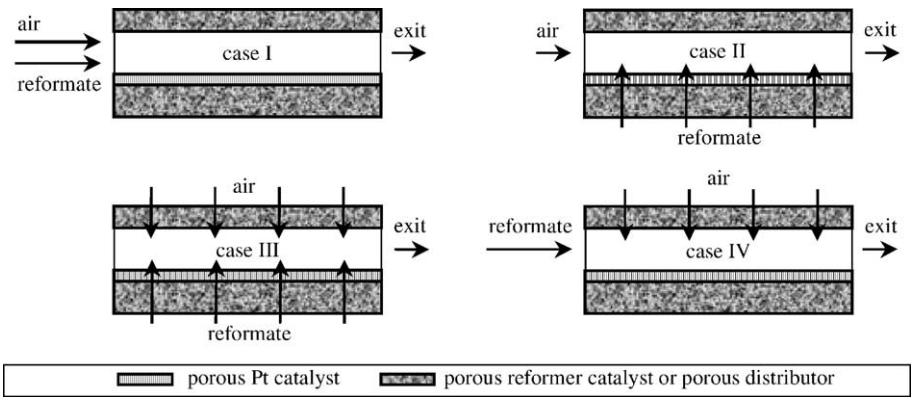

Fig. 6. Cases of contacting patterns for air and reformate in the section of CO-oxidation.

(4) is the desired oxidation of CO in order to produce CO-free (<40 ppm) reformate for a fuel cell. Reaction (5), the undesired side reaction of O_2 with already generated H_2, always occurs because of the limited selectivity (about 50%) of the Pt-catalyst. The RWGS reaction (6) is responsible for CO formation, especially at low CO concentrations and high temperatures. This side reaction limits the operation temperature and the achievable dynamic range (turn down ratio) of the IFP, as for low loads the oxygen is completely consumed at the front edge of the catalyst surface leaving the following Pt-catalyst reproducing CO via reaction (6).

The quantitative description (9)–(11) of the reaction rates is based on own experimental data taken with differential measurements in the relevant parameter space. For CO and O_2 the range of validity is 10–50 000 ppm. p_i (bar) is the partial pressure of the component i:

$$r_4 = \left[\frac{k_4 p_{CO}}{1 + K_{CO} p_{CO}} - k_{inh} p_{CO}\right] p_{O_2}^{0.5} \quad (9)$$

$$r_5 = k_5 p_{CO}^{-0.33} p_{O_2}^{0.5} \quad (10)$$

$$r_6 = \frac{1}{k_{6a} + k_{6b} p_{CO}^{1.5}} \quad (11)$$

The rate equation for CO-oxidation (9) is based on the Langmuir–Hinshelwood mechanism. It was empirically extended by another inhibition term to fit our experimental data. This corresponds to a negative reaction order for p_{CO}, that is reported by several authors in [14]. The rate equation for H_2 oxidation (10) is valid for high H_2 mole fractions (>40%). Because of the large excess of H_2 there is no dependence on p_{H_2} and the latter is part of the rate constant. Further the negative reaction order of p_{CO} represents the strong adsorption of CO on Pt that hinders H_2 oxidation. The reaction rate of the RWGS (11) depends mainly on p_{CO}, because H_2, CO_2 and H_2O are available in abundance. Again the reaction is hindered by CO blocking the surface.

The constants are given for the temperature of 300 °C:

$$k_4 = 1.74 \times 10^4\ \mathrm{mol/(s\,g_{Pt}\,bar^{1.5})},$$
$$k_5 = 0.0353\ \mathrm{mol/(s\,g_{Pt}\,bar^{0.17})},$$
$$K_{CO} = 10^5\ \mathrm{bar^{-1}}, \qquad k_{6a} = 905\ \mathrm{mol/(s\,g_{Pt})},$$
$$k_{inh} = 0.521\ \mathrm{mol/(s\,g_{Pt}\,bar^{1.5})},$$
$$k_{6b} = 35.1 \times 10^6\ \mathrm{s\,g_{Pt}/(mol\,bar^{1.5})}$$

The rate expressions were determined for partial pressure on the catalyst surface. Therefore mass transport from the bulk of the gas phase to the surface of the catalyst has to be considered for CO and O_2 while all other components are available in excess. This means the introduction of two algebraic equations

$$\rho_{cat}(r_4 - r_6) = \beta_{CO} \frac{1}{RT}(p_{CO,bulk} - p_{CO}) \quad (12)$$

$$\rho_{cat}(r_4 + r_5) = \beta_{O_2} \frac{2}{RT}(p_{O_2,bulk} - p_{O_2}) \quad (13)$$

into the model, with β_i denoting the mass transfer coefficient of component i ($\mathrm{m\,s^{-1}}$), R the gas constant and $p_{i,\,bulk}$ and p_i are the partial pressures of component i in the bulk and on the catalyst surface. The mass transfer coefficients were obtained from Sherwood correlations for laminar flow in rectangular channels [15]. The approach is suitable for Reynolds numbers below 500 and small CO and O_2 concentrations, which is valid for the application here. For case II and III, where CO rich reformate flows through the catalyst the mass transport resistance for CO can be neglected. However, variations of β_i have shown this procedure to be suitable for qualitative statements. For quantitative predictions more efforts are necessary, e.g. two-dimensional modelling of the flow.

To carry out simulation, reactor conditions and feed composition must be defined. Therefore an isotherm operation at 300 °C at a pressure of 1.5 bar is assumed. In all cases the reformate stream contains 1% of CO. The total molar flux of O_2 was chosen to be twice the mole flux of CO in the reformate. The catalyst density was $1\ \mathrm{g_{Pt}\,m^{-2}}$ for all cases, leading to reasonable conversions of CO for the given feed rate of methanol.

5.2. Results and discussion

Results of the simulation are presented in Fig. 7, where CO concentrations of the product stream are shown in dependence on the product flow of hydrogen leaving the IFP (equivalent to load).

Discussion of the results starts with the reference case I. At high loads the reactor is overloaded and CO emissions are high. Reducing load leads to a minimum

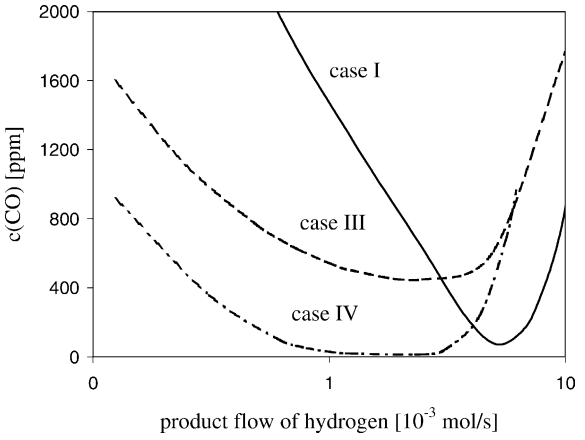

Fig. 7. Simulated product concentration of CO as a function of load for different contacting patterns of reformate and air (feed concentrations: $c(CO) = 1\%$ and $c(O_2) = 2\%$, $T = 300\,^{\circ}C$, $p = 1.5$ bar(a)).

of CO concentration (about 80 ppm) in the product stream. Further decrease of the load results in complete O_2 conversion before the end of the reactor. The absence of O_2 makes it impossible to oxidise CO that is formed due to the RWGS reaction. Consequently, the RWGS reaction is responsible for increasing CO emissions at decreasing loads. In Fig. 7 this is the zone on the left side of the minimum.

Case II is not suitable for the reduction of CO emissions and the minimum is higher than 4000 ppm (not shown in Fig. 7). The reason for this behaviour is unselective O_2 conversion to water (Eq. (5)) at the inlet section of the reactor, where the O_2/CO ratio is very high.

For case III, the minimum CO emissions are higher than for case I. On the other hand, the slope at low loads is not that steep. Consequently, larger load variations respectively a higher turn down ratio can be obtained when exit concentrations of CO >600 ppm are accepted (another stage of CO-oxidation has to follow downstream). A further aspect not obvious in Fig. 7 is that here the rates are constant over the length of the reactor. As a consequence we have an evenly distributed heat production on the reverse side of the reforming section.

Case IV should be favoured when minimum CO emissions are desired. Further the side feed of O_2 offers the possibility for a large dynamic range with very low emissions.

To conclude the discussion, the side feed of O_2 is associated with significant advantages concerning performance in selective oxidation and heat distribution. The combination case III followed by case IV, for instance, appears to be favourable [16].

6. Conclusions and outlook

For the conversion of liquid methanol to a reformate for fuel cells it was shown, that the series of necessary process steps can be integrated into one monolithic reactor. The experimental results proved the simple control of the unit and the excellent temperature distribution. Especially the incorporation of the vaporiser and the feasibility of the start-up using liquid feed were successfully demonstrated.

The chosen power level falls between portable and residential as well as industrial applications. Both up and down scaling of the concept are possible due to the modular design and the adaptable size of the plates. For the low power region, the compactness and ease of control make the system competitive to DMFC-systems.

The fuel processor is a first prototype, which shows various directions for optimisation of manufacturing and process. The observed small MeOH-bypass will be tackled by modifications in design and manufacturing. Lifetime has to be proved further, especially for the region of phase transition. Dependent on application, other features like time for start-up or pressure drop can be addressed. The results of computer modelling indicate, that other contacting patterns of air with reformate offer considerable improvements: the CO concentration in the product can be reduced, meanwhile the dynamic range can be extended.

The IFP can be regarded as an example, how techniques from powder metallurgy can be applied to process integration. Like the known, mostly smaller scale microreactors, the IFP establishes short distances for heat and mass transfer and avoids maldistribution. In addition to the known advantages of microreactors like uniform process conditions, the powder technology offers new appealing possibilities for the design of reactors. Multifunctionality can be achieved. One plate can consist of porous, catalyst carrying sections, tight edge sections, as well as mixing sections which function like corrugated steel plates. As the joining

takes place at moderate temperatures, complex structures with sensitive catalysts can be shaped before assembly of the stack.

The possibility to flow through a porous plane in perpendicular direction enables new contacting patterns of feed streams and process combinations. The technique of fixing the catalyst in a structural supporting matrix can be applied to many other cases, because the mechanical fixing only requires sufficient stability of the catalyst powder. As far as product cost is concerned, we use low cost material and technologies which are applicable for high volume production.

References

[1] G. Ruselowski, Argonne National Laboratory, BP, Exxon Mobil, Shell, GM, Well-to-Whell Energy Use and Greenhouse Gas Emissions of Advanced Fuel/Vehicle Systems, 2001. http://www.transportation.anl.gov/ttrdc/publications/index.html.
[2] DaimlerChrysler, Publication: Necar 5—driving with methanol, 2000.
[3] German Patent 19 853 379 (1998).
[4] M. Schüssler, Fortschritt-Berichte Reihe 6, Nr. 401, VDI-Verlag, Dusseldorf, 1998.
[5] M. Schüssler, et al., Chem. Eng. Technol. 24 (11) (2001) 1141–1145.
[6] W. Ehrfeld, et al., Microreactors: New Technology for Modern Chemistry, Wiley/VCH, Weinheim, 2000.
[7] V. Hessel, H. Löwe, Chemie Ingenieur und Technik 74 (2002) 185–207.
[8] US Patent 5 534 328 (1996).
[9] P. Reuse, et al., in: Proceedings of the Fifth International Conference on Microreaction Technology, Strasbourg, 2001.
[10] B. Willer, Elektrische Leitfähigkeit und Dilatation bei Sintervorgängen, Ph.D. Thesis, Universität GH Kassel, 1984.
[11] German Patent 19 944 187 (1999).
[12] German Patent 10 046 692 (2000).
[13] German Patent 10 039 592 (2000).
[14] M.J. Kahlich, H.A. Gasteiger, R.J. Behm, J. Catal. 171 (1997) 93–105.
[15] R. Jeschar, R. Alt, E. Specht, Grundlagen der Wärmeübertragung, 3, Auflage, Viola-Jeschar-Verlag, Goslar, 1990.
[16] German Patent 10 214 293.3 (2002).